BRAIN
ORIGINAL ARTICLE

Cation leak underlies neuronal excitability in an HCN1 developmental and epileptic encephalopathy

Lauren E. Bleakley,[1] Chaseley E. McKenzie,[1] Ming S. Soh,[1] Ian C. Forster,[1] Paulo Pinares-Garcia,[1] Alicia Sedo,[1] Anirudh Kathirvel,[1] Leonid Churilov,[1,2] Nikola Jancovski,[1] Snezana Maljevic,[1] Samuel F. Berkovic,[3] Ingrid E. Scheffer,[1,3,4] Steven Petrou,[1] Bina Santoro[5] and Christopher A. Reid[1,3]

See Shah (doi:10.1093/brain/awab220) for a scientific commentary on this article.

Pathogenic variants in *HCN1* are associated with developmental and epileptic encephalopathies. The recurrent *de novo* HCN1 M305L pathogenic variant is associated with severe developmental impairment and drug-resistant epilepsy.

We engineered the homologue Hcn1 M294L heterozygous knock-in ($Hcn1^{M294L}$) mouse to explore the disease mechanism underlying an *HCN1* developmental and epileptic encephalopathy.

The $Hcn1^{M294L}$ mouse recapitulated the phenotypic features of patients with the HCN1 M305L variant, including spontaneous seizures and a learning deficit. Active epileptiform spiking on the electrocorticogram and morphological markers typical of rodent seizure models were observed in the $Hcn1^{M294L}$ mouse. Lamotrigine exacerbated seizures and increased spiking, whereas sodium valproate reduced spiking, mirroring drug responses reported in a patient with this variant. Functional analysis in *Xenopus laevis* oocytes and layer V somatosensory cortical pyramidal neurons in *ex vivo* tissue revealed a loss of voltage dependence for the disease variant resulting in a constitutively open channel that allowed for cation 'leak' at depolarized membrane potentials. Consequently, $Hcn1^{M294L}$ layer V somatosensory cortical pyramidal neurons were significantly depolarized at rest. These neurons adapted through a depolarizing shift in action potential threshold. Despite this compensation, layer V somatosensory cortical pyramidal neurons fired action potentials more readily from rest. A similar depolarized resting potential and left-shift in rheobase was observed for CA1 hippocampal pyramidal neurons.

The $Hcn1^{M294L}$ mouse provides insight into the pathological mechanisms underlying hyperexcitability in *HCN1* developmental and epileptic encephalopathy, as well as being a preclinical model with strong construct and face validity, on which potential treatments can be tested.

1 Florey Institute of Neuroscience and Mental Health, University of Melbourne, Parkville, Victoria 3052, Australia
2 Melbourne Medical School, University of Melbourne, Parkville, Victoria 3010, Australia
3 Department of Medicine, Epilepsy Research Centre, University of Melbourne, Austin Health, Heidelberg, Victoria 3084, Australia
4 Department of Paediatrics, University of Melbourne, Royal Children's Hospital, Parkville, Victoria 3052, Australia
5 Department of Neuroscience, The Kavli Institute for Brain Science, Mortimer B. Zuckerman Mind Brain Behavior Institute, Columbia University, New York, NY 10027, USA

Received September 4, 2020. Revised February 12, 2021. Accepted March 20, 2021. Advance access publication April 1, 2021

Correspondence to: Christopher A. Reid
Florey Institute of Neuroscience and Mental Health
University of Melbourne, Parkville, Victoria 3010, Australia
E-mail: careid@unimelb.edu.au

Keywords: epilepsy; HCN channels; genetic mouse model; ion channel; developmental and epileptic encephalopathy

Abbreviations: AP = action potential; DEE = developmental and epileptic encephalopathy; ECoG = electrocorticography; HCN channel = hyperpolarization-activated cyclic nucleotide-gated channel; I_h = hyperpolarization-activated current; Rm = input resistance; RMP = resting membrane potential; sPSC = spontaneous postsynaptic current

Introduction

Epilepsy is a disorder characterized by an enduring predisposition to generate recurrent, unprovoked seizures, which occur due to neuronal hyperexcitability and hypersynchronous firing.[1] Although the epilepsies have diverse underlying aetiologies, a significant proportion have a genetic basis.[2] Many genes implicated in epilepsy encode voltage-gated or ligand-gated ion channels (reviewed in Oyrer *et al.*[3]). Hyperpolarization-activated, cyclic nucleotide-gated channels (HCN channels) are one such ion channel family that is associated with epilepsy.[4–10] HCN channels are encoded by *HCN1*, *HCN2*, *HCN3* and *HCN4*, with each subtype having distinct expression profiles, kinetics, activation voltages, and sensitivity to modulation by cyclic AMP.[11]

The HCN1 subtype has the strongest association with epilepsy, with several *de novo* variants reported in patients with developmental and epileptic encephalopathy (DEE).[4–6,12] DEEs are characterized by drug-resistant seizures, an epileptiform EEG, and developmental slowing and often regression.[13] Specific genetic DEEs are associated with prominent fever sensitivity, such as Dravet syndrome and *HCN1* DEE. More recently, the spectrum of HCN1-based epilepsies has expanded to encompass milder syndromes including genetic epilepsy with febrile seizures plus (GEFS+), which can arise due to *de novo* or inherited variants.[5,14] Disease severity depends on the location of the variant, with those causing DEE tending to be within the transmembrane domains, and those outside more likely to cause milder syndromes.[5]

HCN channels are non-selective cation channels that are expressed throughout the CNS. They are opened by membrane hyperpolarization and pass a current termed I_h.[11] At rest, I_h comprises an inward, depolarizing conductance carried primarily by sodium. The unique activation profile of HCN channels enables I_h to play critical roles in modulating dendritic excitability, contributing to setting the resting membrane potential (RMP) of neurons, and regulating rhythmic, pacemaker activity.[11] Functional analysis in expression systems revealed that *HCN1* pathogenic variants associated with epilepsy cause a diverse range of changes to biophysical properties including channel current density, activation and deactivation kinetics, and voltage dependence,[5,6] with both loss and gain of channel function reported.[5] This highlights a recognized complex relationship between changes in HCN channel function and epilepsy, with both increases and decreases in I_h correlating with hyperexcitability.[15,16] It also underlines the difficulty in ascribing pathogenic cellular and network mechanisms to changes observed in simple expression systems. Here we address this challenge by engineering and characterizing a knock-in mouse model based on the HCN1 M305L *de novo* variant that causes DEE.[5]

The HCN1 M305L variant is located in the S5 transmembrane domain of the protein and has been identified in two unrelated patients with DEE.[5] Here we show that the homologue Hcn1 M294L heterozygous knock-in ($Hcn1^{M294L}$) mouse has spontaneous seizures, hyperexcitable electrocorticographic (ECoG) activity, morphological markers consistent with seizures, pharmacosensitivity mirroring that observed in an *HCN1* DEE patient, and distinct behavioural changes. Functional analysis reveals that the HCN1 M305L variant causes a loss of voltage dependence, resulting in a constitutively open cation 'leak' channel. As a consequence, layer V and CA1 pyramidal neurons have depolarized RMPs and fire action potentials (APs) more readily, providing a mechanistic explanation for how HCN1 channel dysfunction can lead to neuronal hyperexcitability and therefore epilepsy.

Materials and methods

Animals

Generation of the $Hcn1^{M294L}$ mouse model

A guide RNA target site close to amino acid 294 of the mouse *Hcn1* gene was identified using the UCSC Genome Browser (https://genome.ucsc.edu/ Accessed 22 June 2021). The guide RNA sequence used was 5′-GAAGCAGCATCATGCCAATG-3′. CRISPR RNA (crRNA, Integrated DNA Technologies) was annealed with trans-activating crRNA (tracrRNA) to form a functional crRNA:tracrRNA guide RNA duplex. Cas9 nuclease (Integrated DNA Technologies) was incubated with the guide RNAs to form a ribonucleoprotein (RNP) complex. A single stranded repair oligo containing the desired amino acid change (Integrated DNA Technologies) was used as a repair template. The C147-HCN1-M294L repair template sequence was 5′-TGCTGACAGATATTCCACATGACCTATGACCTCGCCAGTGCTGTGGTGAGGATCTTCAACCTCATCGGAATGTTGCTGCTTCTGTGCCACTGGGATGGCTGTCTTCAGTTCCTGGTTCCCCTGCTGCAGGACTTCCCA-3′. Cas9 nuclease (30 ng/μl), the RNPs (30 ng/μl) and the ssDNA homology directed repair template (30 ng/μl) were microinjected into the pronucleus of C57BL/6J zygotes at the pronuclei stage. Injected zygotes were transferred into the uterus of pseudopregnant F1 females.

Animal housing and husbandry

Mice were bred on-site at the Florey Institute of Neuroscience and Mental Health. Male heterozygous $Hcn1^{M294L}$ mice were mated with wild-type C57BL/6J female mice, yielding either $Hcn1^{+/+}$ (wild-type) or $Hcn1^{M294L/+}$ ($Hcn1^{M294L}$) offspring. Mice were housed in standard 15 × 30 × 12 cm cages maintained under 12-h dark and light cycles, with access to dry pellet food and tap water *ad libitum*. For all experiments both male and female mice were used, with littermates used wherever possible.

Ethics and animal welfare

Experiments were performed in accordance with the Prevention of Cruelty to Animals Act, 1986 under the guidelines of the National Health and Medical Research Council (NHMRC) of Australia Code of Practice for the Care and Use of Animals for Experimental Purposes. All experiments were approved by the Animal Ethics Committee at the Florey Institute of Neuroscience and Mental

Health prior to commencement. Animals were monitored in line with protocols approved by this committee. Anaesthesia and analgesia were used where appropriate. Mice were acclimatized to experimental rooms for at least 30 min before experimentation. At the conclusion of experimentation mice were culled by cervical dislocation or decapitation following deep isoflurane anaesthesia, which are ANZCCART approved methods.

Statistical analysis

Spontaneous postsynaptic current (sPSC) data were analysed using multi-level regression analyses performed using Stata software (Supplementary material). All other statistical analyses were performed using GraphPad Prism software (version 8.1.0–8.3). Data are reported and plotted as mean ± standard error of the mean (SEM). Oocyte data are reported in the absence of further statistical analysis. Baseline survival, thermogenic seizure susceptibility and subcutaneous pentylenetetrazole (PTZ) seizure susceptibility were each analysed using a Mantel-Cox log-rank test. Statistical analyses used for behavioural data are listed in Supplementary Table 1. Numerical values for electrophysiology data including mean, standard error and *P*-values are reported in Supplementary Table 2. Other data were first analysed using a Shapiro-Wilk test for normality. Statistical significance was then determined using a two-tailed Student's *t*-test (paired or unpaired as appropriate) for normally distributed data, or a Mann-Whitney U-test for unpaired data where the Shapiro-Wilk test returned a result of <0.05. Statistical significance was set at $P < 0.05$.

Transcardial perfusions and immunohistochemistry

$Hcn1^{M294L}$ and wild-type mice [postnatal Day (P)99–P113] were transcardially perfused (Supplementary material) and 40 μm coronal slices cut from fixed brains. Slices were assayed for HCN1, neuropeptide Y (NPY) and glial fibrillary acidic protein (GFAP) expression, as well as gross morphology using Nissl staining. Details of the antibodies and stains used, incubation protocols, and acquisition of fluorescence images can be found in the Supplementary material.

Electrocorticography

Electrocorticography electrode implantation surgery and recordings

A detailed outline of the ECoG electrode implantation surgery and set-up for recordings can be found in the Supplementary material. ECoG data were sampled at 250 Hz and filtered (40 Hz low-pass, 0.5 Hz high-pass) using Sirenia Acquisition software (version 2.1.0, Pinnacle Technology Inc.). Twenty-four-hour recordings were conducted to characterize baseline EEG activity. For drug studies, baseline ECoG activity was recorded for 2 h, before mice were administered sodium valproate (200 mg/kg, dissolved in 0.9% w/v saline), lamotrigine (isethionate salt, 20 mg/kg, dissolved in 0.9% w/v saline) or vehicle control intraperitoneally (30G needle), and then ECoG activity was recorded for a further 2 h. Mice were exposed to multiple drugs, with at least 48 h between any two drug administrations. Any mice that had seizures following lamotrigine administration were culled at the conclusion of that recording. All ECoG recordings where drugs were administered were conducted during the light phase of the light-dark cycle.

Spike counting

Spike analysis was performed by visual inspection of raw ECoG data visualized and extracted using Sirenia Seizure Pro software (version 1.7.5, Pinnacle Technology Inc.). 'Spikes' had distinctive morphology (Fig. 2A) and were defined as biphasic events lasting <200 ms with at least thrice the amplitude of baseline ECoG activity. Spikes in 1 h were counted to study underlying epileptiform activity. For drug studies, spikes were counted in two 1 h segments: immediately before drug administration, and from 10 to 70 min following drug administration (or, for mice which had seizures following lamotrigine, from 10 min post-injection until seizure commencement). All spike analyses were completed by a blinded experimenter.

Seizure susceptibility assays

Thermogenic seizure assay

Mice (P17) were divided into genotypes, paired based on weight, and placed into an enclosed chamber heated to $42 \pm 1^{\circ}C$ for a maximum of 20 min to induce seizures modelling febrile seizures, as previously described.[17] Mice were culled by cervical dislocation immediately following a terminal seizure. Time at death was recorded.

Subcutaneous pentylenetetrazole assay

Mice (P32–P37) were injected subcutaneously with 80 mg/kg PTZ and monitored for a maximum of 30 min. Time to first tonic-clonic seizure was recorded. Mice were culled by cervical dislocation after 30 min.

Behavioural assays

Behavioural differences between $Hcn1^{M294L}$ and wild-type mice were assessed using: open-field locomotor assay, rotarod, ledged beam, light-dark box assay, elevated plus maze, Y-maze, Barnes maze, and a three-chamber social interaction assay. Details of each of these assays can be found in the Supplementary material.

Oocyte electrophysiology

Details of the site-directed mutagenesis, cRNA preparation, oocyte preparation and injection protocols as well as solutions and reagents used can be found in the Supplementary material.

Standard two-electrode voltage clamp hardware was used (TEC-05X or TEC10X, NPI), with series resistance (R_s) compensation applied to ensure clamp accuracy. Electrodes were filled with 3M KCl and had resistances between 0.5 and 1.5 MΩ. Voltage clamp control, data acquisition and perfusion valve switching were under software control (pCLAMP version 8–10, Molecular Devices). All experiments were performed at 18–20°C. Current-voltage (*I–V*) curves were generated using a voltage step protocol with 10 mV steps lasting 2.5 s from a –30 mV holding potential to test potentials in the range –120 mV to +20 mV. Steady-state current was measured over a ~200 ms interval at the end of the test pulse. Data were sampled at 200 μs/point and low pass filtered at 500 Hz. Curve fitting of the activation kinetics was performed using Clampfit routines.

Slice electrophysiology

Details of the solutions and reagents used and of the slice preparation procedure can be found in the Supplementary material. Electrophysiology was conducted on tissue from mice aged P26–P62 (wild-type mean age = P46, $Hcn1^{M294L}$ mean age = P45).

Slices were mounted in a recording chamber and continually perfused with artificial CSF bubbled with carbogen gas (2 ml/min) at a bath temperature of 32°C. Whole-cell patch clamp recordings from layer V somatosensory cortical pyramidal neurons (layer V neurons) and CA1 hippocampal pyramidal neurons (CA1 neurons) were made using borosilicate glass electrodes with initial resistance of 3–7 MΩ. Recordings were made using an Axon Multiclamp 700B amplifier (Molecular Devices), Digidata 1550 digitizer (Molecular Devices), and

pCLAMP version 10 software. Data were sampled at 50 kHz with a low-pass filter at 10 kHz. All slice electrophysiology data were analysed using AxoGraph X (version 1.7.6).

I–V curves were generated from layer V neurons in voltage clamp mode using a protocol with 5 mV steps lasting 2 s from a –50 mV holding potential to test potentials in the range –100 mV to –45 mV. Steady-state currents were measured over a 500 ms interval at the end of the test pulse to construct the *I–V* relationship. To isolate I_h, ZD 7288 (20 μM) was added to the artificial CSF and washed on for at least 5 min. Traces were normalized to the holding potential (–50 mV) and post-ZD 7288 traces were subtracted from corresponding pre-ZD 7288 recordings. Input resistance (Rm) was calculated from holding potentials of –70 mV and –50 mV using –10 mV test pulses. SPSCs were detected in voltage clamp gap-free recordings conducted at –70 mV using a sliding template as previously described.[18] Reported currents are not corrected for junction potential offset.

All other slice electrophysiology data were collected in current clamp. Bridge balance and pipette capacitance neutralization were manually applied. Current injection-AP output (*i-o*) relationships were established using a step protocol of 2 s square pulses from –100 pA to +400 pA in 25 pA steps, which was conducted both from rest and from –70 mV. Input-output curves were constructed from raw numbers of events automatically detected in AxoGraph using an amplitude threshold of at least 60 mV. AP morphological characteristics were obtained from the first AP at rheobase. Threshold was defined as the voltage at which the rising membrane potential slope exceeded 10 mV/ms. Amplitude was defined as the AP peak relative to a normalized baseline averaged from 0 ms to 10 ms before threshold. Rise time was defined as the time from 10% to 90% of peak. Width was measured at 50% of peak height. Decay time was defined as the time from 100% to 50% of peak. Gain was calculated by measuring the area under the curve across 15 sequential sweeps beginning with the sweep immediately before rheobase. Rm from rest was calculated in current clamp by measuring voltage change from baseline to current onset in the –50 pA, –25 pA and 0 pA sweeps of the *i-o* protocol. Values were fitted by linear regression and the gradient used to estimate Rm.

Sag was elicited in layer V neurons with a –100 pA current injection and from CA1 neurons with a –250 pA current injection, both from a –70 mV holding potential. Sag was defined as the difference between the most hyperpolarized point within the first second and the final 'steady state' of the voltage trace. Gap-free recordings in the absence of holding current were conducted to measure RMP. Cells that spontaneously fired APs were excluded from current clamp analyses (n = 5 wild-type, n = 4 $Hcn1^{M294L}$). In a subset of cells, RMP was also recorded in the presence and absence of ZD 7288 (20 μM) washed on for at least 5 min. In a separate set of experiments, AP5, NBQX and picrotoxin (each at 10 μM) were added to the artificial CSF and washed on for at least 5 min to block synaptic activity.

Quantitative reverse transcription PCR

Quantitative reverse transcription PCR (RT-qPCR) was performed on cortical tissue from mice aged P52–P58, using mouse-specific probes to the genes *Scn2a*, *Scn8a*, *Hcn1*, *Hcn2*, and the mouse endogenous gene *Gusb*. Details of the RNA isolation, purification and analysis processes, as well as the particular probes used, can be found in the Supplementary material.

Data availability

Raw data and images are available upon request from the corresponding author.

Results

Phenotype of *HCN1* developmental and epileptic encephalopathy due to the M305L pathogenic variant

Two unrelated patients with DEE caused by the *de novo* HCN1 M305L pathogenic variant have been reported.[5] Patient 10 from that study is now 4 years old. She first presented with an afebrile tonic-clonic seizure in the setting of a viral infection at age 12 weeks. Her epilepsy escalated up to 20 afebrile tonic-clonic seizures per day. Valproate controlled seizures after the following medicines failed: topiramate, phenobarbitone, vigabatrin, clonazepam, pyridoxine and levetiracetam. Lamotrigine increased seizure frequency. She continued to have seizure clusters with viral illnesses, typically triggered by low-grade fever (high 37°C to 38°C). She had two episodes of convulsive status epilepticus: at 5 months and 3 years. By 3.5 years, she had predominantly febrile tonic-clonic seizures, but also myoclonic seizures, rare focal seizures and possible atonic head nods. Her EEG showed multifocal epileptiform activity with focal seizures emanating from the right and left centrotemporal regions independently. A subclinical left frontal seizure in sleep was also recorded. Her brain MRI was normal at 3 months.

Her development was never normal. By 3.5 years, she had severe global impairment and could walk in a walker, speak seven single words, and follow a single command. She had likely cortical visual impairment, bilateral hearing impairment associated with recurrent otitis media, stereotypies, central sleep apnoea from age 6 months following laryngomalacia in infancy, and recurrent aspiration pneumonia.

$Hcn1^{M294L}$ mice display an epileptic phenotype

To study the role of the HCN1 M305L variant in DEE, we generated the homologue $Hcn1^{M294L}$ mouse model. *HCN1* DEE patients carry heterozygous mutations,[5] rendering the heterozygous $Hcn1^{M294L}$ mouse a molecular correlate of the human condition. Heterozygous $Hcn1^{M294L}$ mice were born with an approximate Mendelian ratio suggesting no excess embryonic lethality occurred. We were unable to generate homozygous $Hcn1^{M294L}$ mice as female $Hcn1^{M294L}$ mice did not fall pregnant.

$Hcn1^{M294L}$ mice were significantly smaller than wild-type littermates (Fig. 1A and B). There were no differences between $Hcn1^{M294L}$ and wild-type mice in brain size or gross brain morphology based on a qualitative analysis (Fig. 1C). Spontaneous seizures were observed in $Hcn1^{M294L}$ mice, although these were rare (Supplementary Video 1). $Hcn1^{M294L}$ mice also showed a small increase in propensity to sudden unexpected death which occurred over ages ranging from P23 to P317 (19 instances of sudden death in $Hcn1^{M294L}$ mice, two in wild-type mice), with a statistically significant increase in deaths from P21 to P30 (Fig. 1D). Several $Hcn1^{M294L}$ mice were found dead with hind-limb extension, suggestive of a terminal seizure.[19]

ECoG traces recorded from $Hcn1^{M294L}$ mice displayed large amplitude interictal spikes with a distinct waveform pattern (Fig. 2A), which were absent from recordings of wild-type mice (Fig. 2B). Given the low number of spontaneous seizures in $Hcn1^{M294L}$ mice, we used the frequency of these ECoG spikes as a quantifiable marker of excitability. Consistent with observed efficacy in a patient with HCN1 DEE, sodium valproate caused a significant decrease in ECoG spike frequency in $Hcn1^{M294L}$ mice (Fig. 2C and D). Lamotrigine caused a significant increase in ECoG spike frequency and, in 6 of 11 mice tested, induced at least one full tonic-clonic seizure (Racine class 4 or 5)[20] within 70 min of administration (Fig.

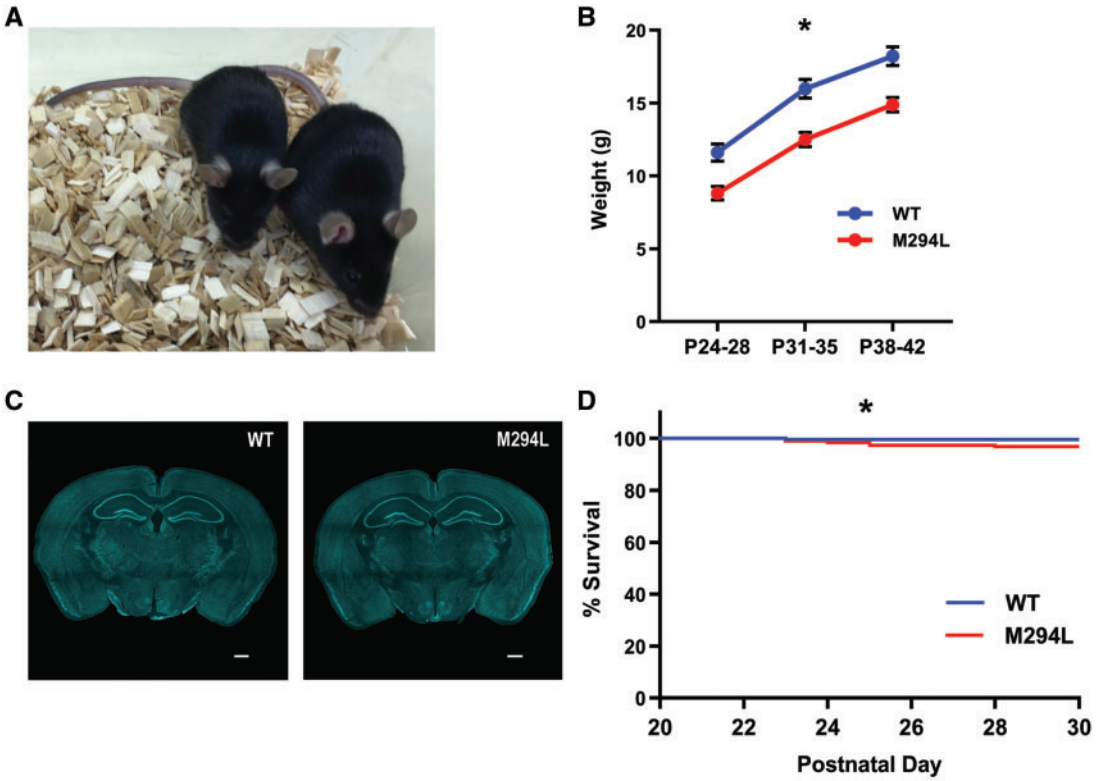

Figure 1 Size and survival of Hcn1^{M294L} mice. (**A**) Hcn1^{M294L} mice (*left*) were significantly smaller than their wild-type (WT) littermates (*right*). (**B**) Body weight of Hcn1^{M294L} mice and wild-type littermates over three time points in the 3 weeks post-weaning (n = 17 wild-type, 16 Hcn1^{M294L}). *$P < 0.001$ for all three time points. (**C**) Nissl staining of whole brain slice from wild-type (*left*) and Hcn1^{M294L} (*right*) mouse (scale bar = 520 μm). (**D**) There was a significant difference in survival of wild-type and Hcn1^{M294L} mice between weaning and P30 (n = 221 wild-type, 192 Hcn1^{M294L}), *$P = 0.04$ (Mantel-Cox log-rank test).

2E and F), recapitulating the seizure exacerbation observed in the patient (outlined in the previous section).

Molecular markers commonly seen in epilepsy models were distinctly increased in Hcn1^{M294L} mice. These include the upregulation of GFAP, a marker of gliosis,[21] in the hippocampus and parts of the cortex (Fig. 2G and H), and notable upregulation of NPY in hippocampal dentate gyrus mossy fibres (Fig. 2H), a hallmark of temporal lobe epilepsy.[22] In the dentate gyrus, we observed structural alterations compatible with those seen in mesial temporal sclerosis, such as widening of the granule cell layer (granule cell dispersion), expansion of the hilus, and mild gyrification particularly of the suprapyramidal blade (Fig. 2H).[23,24]

Given the propensity for patients with *HCN1* epilepsy to experience febrile seizures,[5] we tested susceptibility to thermogenic seizures. Hcn1^{M294L} mice developed terminal tonic-clonic seizures significantly earlier than wild-type littermates in the thermogenic seizure assay (Fig. 2I). Hcn1^{M294L} mice were also more sensitive to proconvulsant seizures, with a significantly reduced latency to first tonic-clonic seizure in the subcutaneous PTZ assay (Fig. 2J).

Behavioural phenotype of the Hcn1^{M294L} mouse

Hcn1^{M294L} mice were notably more hyperactive than wild-type littermates, both when undisturbed and on handling. Consistent with this observation, Hcn1^{M294L} mice travelled significantly further in an open-field locomotor assay (Fig. 3A), outperformed wild-type littermates in the rotarod assay, and traversed the ledged beam significantly faster, with no significant differences in foot-faults (Supplementary Table 1).

To address if the Hcn1^{M294L} mice modelled developmental delay, we used two memory assays. Interestingly, Hcn1^{M294L} mice performed as well as wild-type littermates on the Y-maze, which probes working memory (Fig. 3B).[25] In contrast, the Hcn1^{M294L} mice underperformed on the Barnes maze test, which probes longer-term spatial reference memory (Fig. 3C).[25]

Results from anxiety assays were mixed. Hcn1^{M294L} mice spent significantly more time in the dark zone of the light-dark box (Fig. 3D) and had a trend towards a reduction in time spent in the centre zone in the open-field locomotor assay (Supplementary Table 1), consistent with increased anxiety. In contrast, results from the elevated plus maze suggested reduced anxiety, with Hcn1^{M294L} mice spending a significantly greater percentage of time in the open arms (Fig. 3E).

We used the three-chamber assay to study social interaction in Hcn1^{M294L} mice. Female, but not male, Hcn1^{M294L} mice displayed a deficit in time spent interacting with a stranger mouse (Fig. 3F). No sex-specific differences in performance were detected in any of the other behavioural assays presented in Fig. 3. Additional behavioural data are presented in Supplementary Table 1. These data highlight that Hcn1^{M294L} mice display clear and significant behavioural differences from wild-type littermates on a range of parameters.

HCN1 M305L ion channels have altered activation kinetics but unchanged cation selectivity

Two-electrode voltage clamp recordings were made from *Xenopus laevis* oocytes to investigate the functional consequences of the M305L variant in human HCN1 channels (Fig. 4A). To mimic the heterozygous situation, a 50:50 mix of wild-type (WT) and M305L cRNA was injected, with total cRNA equal across all conditions.

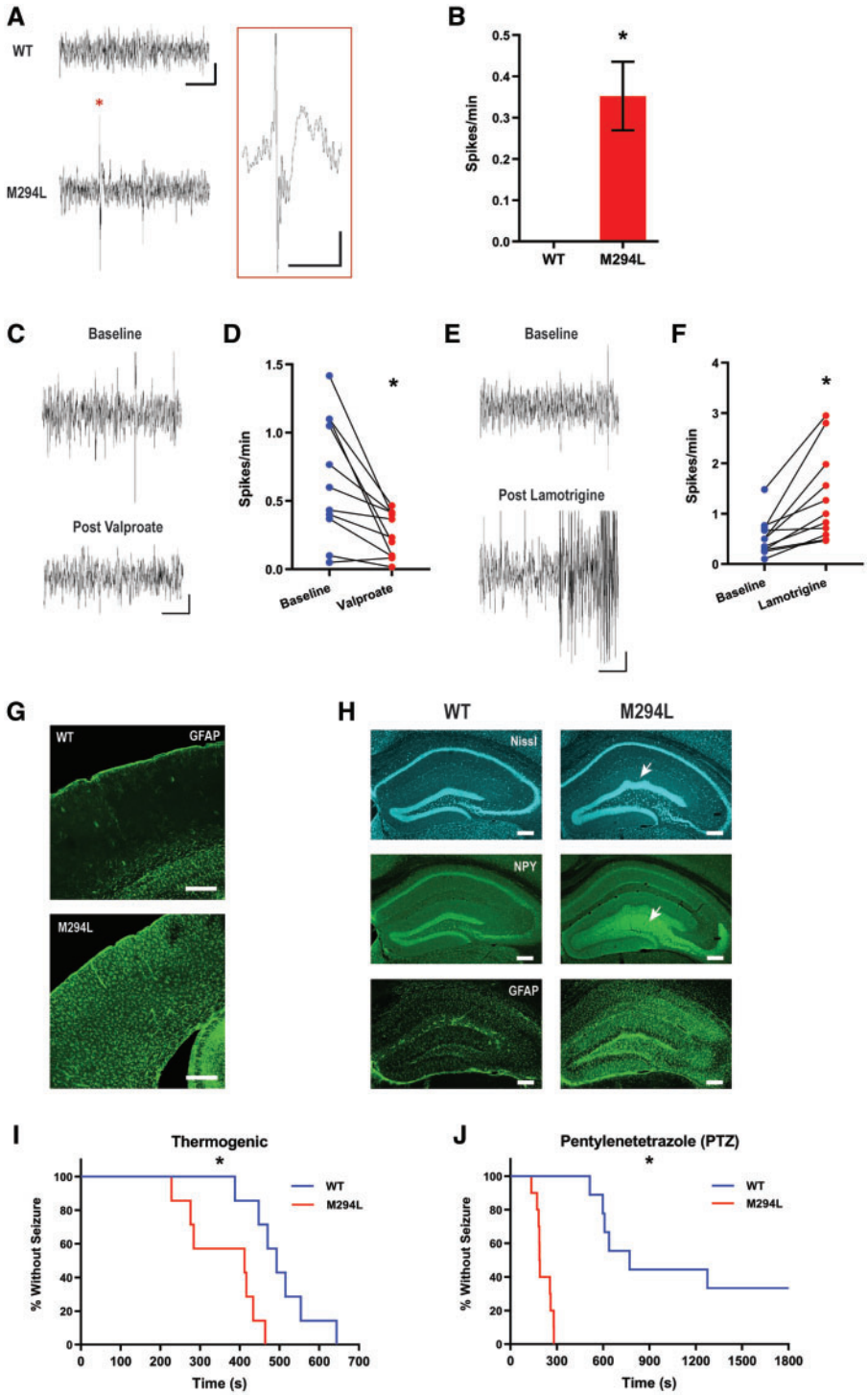

Figure 2 Hcn1^{M294L} mice displayed an epileptic phenotype. (**A**) Sample ECoG traces from a wild-type (WT) (*top*) and an Hcn1^{M294L} (*bottom*) mouse, showing spiking (indicated with an asterisk) in the Hcn1^{M294L} trace (scale bar = 3 s, 90 μV). *Inset*: Expanded view of an Hcn1^{M294L} spike (asterisk) showing epileptiform morphology (scale bar = 500 ms, 90 μV). (**B**) Similar spikes were not seen in ECoG traces from wild-type mice (n = 4 wild-type, 7 Hcn1^{M294L}), *P = 0.01. (**C**) Representative ECoG traces from an Hcn1^{M294L} mouse before (*top*) and after (*bottom*) administration of sodium valproate (200 mg/kg) (scale bar = 3 s, 90 μV). (**D**) Sodium valproate (200 mg/kg) caused a significant decrease in ECoG spike frequency in Hcn1^{M294L} mice (n = 11), *P = 0.005. (**E**) Representative ECoG traces from an Hcn1^{M294L} mouse before (*top*) and after (*bottom*) administration of lamotrigine (20 mg/kg) (scale bar = 3 s, 90 μV). (**F**) Lamotrigine (20 mg/kg) caused a significant increase in ECoG spike frequency in Hcn1^{M294L} mice (n = 11), *P = 0.002. (**G**) GFAP staining of primary somatosensory cortex of a wild-type (*top*) and an Hcn1^{M294L} (*bottom*) mouse, showing gliosis in the Hcn1^{M294L} animal (scale bar = 300 μm). (**H**) Nissl staining showing morphological changes (*top row*, arrow), upregulation of the major epilepsy marker NPY (*middle row*, arrow), and upregulation of the reactive gliosis marker GFAP (*bottom row*) in the hippocampus of Hcn1^{M294L} mice (*right column*) compared to wild-type (*left column*) (scale bar = 250 μm) (n = 6 wild-type, 6 Hcn1^{M294L}). Hippocampal gliosis and upregulation of NPY were seen in 6/6 Hcn1^{M294L} mice and 0/6 wild-type mice. (**I**) Kaplan-Meier curve showing Hcn1^{M294L} mice had a significantly shorter time to terminal seizure in the thermogenic seizure assay compared to wild-type littermates (n = 7 wild-type, 7 Hcn1^{M294L}), *P = 0.004. (**J**) Kaplan-Meier curve showing Hcn1^{M294L} mice had a significantly shorter time to tonic-clonic seizure in the subcutaneous PTZ assay compared to wild-type littermates (n = 9 wild-type, 10 Hcn1^{M294L}), *$P < 0.0001$.

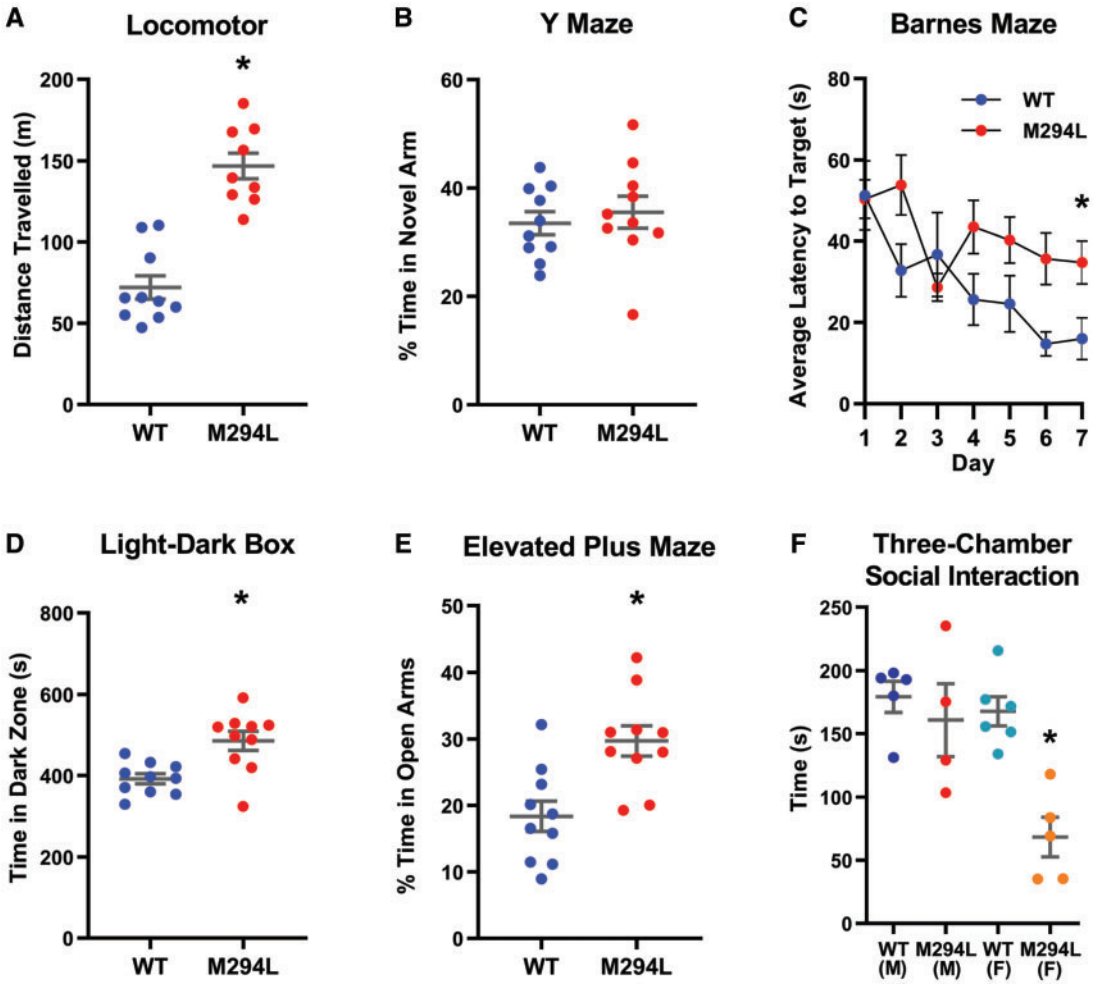

Figure 3 Hcn1^{M294L} mice displayed significant behavioural differences from wild-type littermates. (**A**) Hcn1^{M294L} mice travelled significantly further than wild-type (WT) littermates in the open field locomotor assay over a 60-min period (n = 10 wild-type, 10 Hcn1^{M294L}), *$P < 0.0001$. (**B**) There were no significant differences between genotypes in the percentage of time spent in the novel arm of the Y maze (n = 10 wild-type, 10 Hcn1^{M294L}), $P = 0.6$. (**C**) Hcn1^{M294L} mice showed a significantly increased average latency to target in the Barnes maze assay (n = 10 wild-type, 10 Hcn1^{M294L}), *$P = 0.01$ on Day 7. (**D**) Hcn1^{M294L} mice spent significantly longer in the dark zone of the light-dark box (n = 10 wild-type, 10 Hcn1^{M294L}), *$P = 0.002$. (**E**) Hcn1^{M294L} mice spent significantly longer in the open arms of the elevated plus maze (n = 10 wild-type, 10 Hcn1^{M294L}), *$P = 0.002$. (**F**) Time spent interacting with an age- and sex-matched stranger mouse in the three-chamber social interaction assay. Female, but not male, Hcn1^{M294L} mice showed a deficit in social interaction (n = 5 wild-type males, 6 wild-type females, 4 Hcn1^{M294L} males, 5 Hcn1^{M294L} females), *$P = 0.01$.

Currents at –120 mV for the HCN1 M305L and HCN1 WT + M305L channels were smaller than for HCN1 WT (Fig. 4B and C). HCN1 M305L showed an almost instantaneous change in current in response to voltage steps and an absence of tail currents (Fig. 4B). HCN1 WT + M305L currents showed mixed activation kinetics with an instantaneous component superimposed on a slower activation component. Tail currents were present but, unlike wild-type, also comprised an activating component for depolarizing voltage steps returning to the holding potential (Fig. 4B, arrow). The HCN1 wild-type channel showed strong inward rectification for test potentials below –50 mV.[11] Markedly weaker inward rectification was observed in the HCN1 WT + M305L co-expressed case (Fig. 4D). The activation of the HCN1 WT + M305L channel was also significantly faster and lacked the stronger voltage dependence seen for HCN1 wild-type channels (Fig. 4E).

To test if the cation selectivity of the HCN1 channel had been affected by the M305L variant, external K^+ was substituted with equimolar Na^+, Li^+ or choline (Fig. 4F and G). As expected, substitution of K^+ with Na^+ reduced the current by ~60%[11] with inward rectification still present (Fig. 4F and G). At –100 mV the ratio of currents in 100 K to 100 Na was found to be 0.42 ± 0.05 (n = 6) for wild-type HCN1 and 0.47 ± 0.05 (n = 5) for M305L, strongly suggesting that the ion permeation properties of the pore were unaffected by the variant.

I_h recorded from Hcn1^{M294L} layer V pyramidal neurons lacks voltage dependence

Voltage clamp recordings were conducted in layer V neurons in the absence and presence of ZD 7288 (Fig. 5A). The *I–V* relationship constructed from pre-ZD 7288 traces revealed a more depolarized reversal potential for Hcn1^{M294L} layer V neurons, consistent with the contribution of Na^+ to 'leak' (Fig. 5B). At more hyperpolarized potentials, current amplitudes began to converge as I_h activated in wild-type neurons (Fig. 5B).

ZD 7288 subtracted traces were obtained to better interrogate the biophysical properties of I_h (Fig. 5A). A steady-state *I–V* constructed from subtracted data revealed markedly reduced rectification of I_h at more depolarized potentials in Hcn1^{M294L} neurons (Fig. 5C). Activation kinetics were estimated by fitting a single exponential to the subtracted traces. Activation time constants for I_h in Hcn1^{M294L} neurons were significantly faster than wild-type and

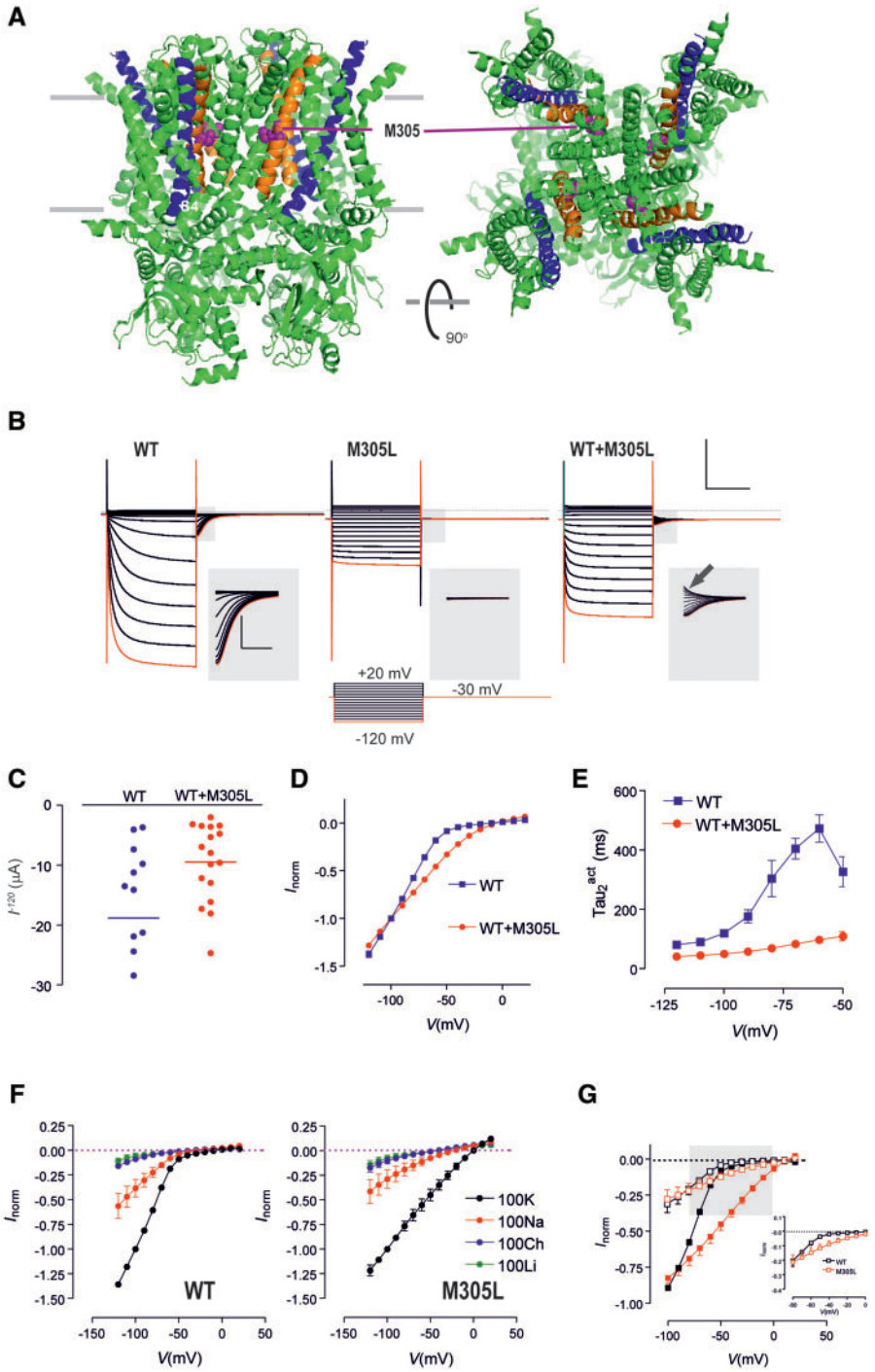

Figure 4 Functional analysis of HCN1 M305L revealed significantly altered activation kinetics but unchanged cation selectivity. (**A**) Structure of human HCN1 showing location of M305 (purple spheres). The S4 helices of the voltage sensing domains are shown in blue and S5 helices shown in orange. Based on PDB 5u60 for human HCN1 in the depolarized (closed) conformation[35] rendered using PyMOL (The PyMOL Molecular Graphics System, Version 2.3.4 Schrödinger, LLC.). (**B**) Representative voltage clamp data from oocytes expressing HCN1 wild-type (WT) (*left*); M305L (*middle*) and co-expressed WT + M305L (*right*) (scale bar = 1 s, 10 μA). Each dataset shows current traces in response to a series of voltage steps (*inset*) from the holding potential (–30 mV) to test potentials in the range –120 mV to +20 mV. Grey shaded boxed areas have been enlarged to show tail currents visible for wild-type and WT + M305L, but absent for M305L (scale bar = 0.1 s, 2 μA). Red trace corresponds to voltage step to –120 mV. Arrow highlights tail current present for depolarizing steps with WT + M305L. (**C**) Average of raw steady-state current for HCN1 WT (n = 14) and WT + M305L (n = 17) measured at end of test pulse to –120 mV. (**D**) Grouped current-voltage (I–V) data normalized to –100 mV shows markedly weaker inward rectification for WT + M305L (n = 4) co-expressing oocytes compared to WT (n = 5). Error bars are smaller than symbols. (**E**) Mean activation time constant τ_2^{act} obtained by fitting the time-dependent component of activating current from wild-type (n = 9) and WT + M305L (n = 10) oocytes with a two-exponential function. (**F**) Normalized I–V data for WT (*left*, n = 6) and M305L (*right*, n = 5) for different external ion substitutions. Data were normalized to the steady-state current in 100 K at –100 mV. Li^+ or choline resulted in much smaller currents, no rectification, and resembled endogenous currents seen in non-injected oocytes (data not shown). (**G**) I–V data from **F** normalized to the steady-state current in 100 K at –100 mV, after subtraction of current in 100 choline. Black symbols = wild-type (n = 10); red symbols = M305L (n = 9). Filled and open symbols are with 100 K superfusion and 100 Na superfusion, respectively. Grey shading represents critical range of potentials for AP initiation and enlarged in inset for 100 Na superfusion.

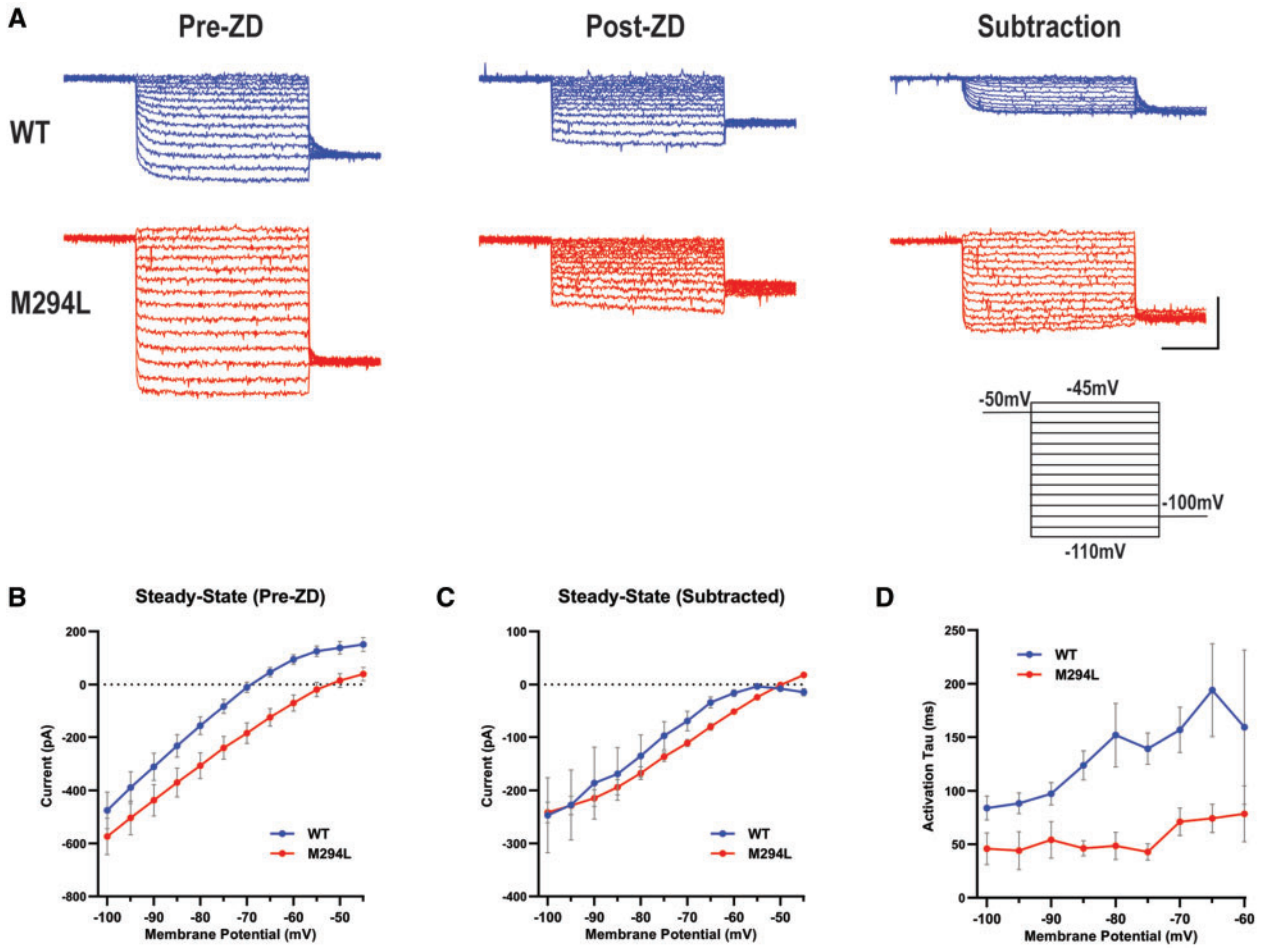

Figure 5 I_h recorded from $Hcn1^{M294L}$ layer V pyramidal neurons lacks voltage dependence. (**A**) Representative voltage clamp data from layer V neurons from wild-type (WT) (blue) and $Hcn1^{M294L}$ (red) mice, at baseline (left, 'pre-ZD'), following the application of ZD 7288 (centre, 'post-ZD'), and I_h isolated by subtracting ZD 7288-sensitive current traces from baseline traces (right, 'subtraction') (scale bar = 1 s, 200 pA). Each dataset shows current traces in response to a series of voltage steps (*inset*) from the holding potential (–50 mV) to test potentials in the range –110 mV to –45 mV. (**B**) Current-voltage (*I–V*) data shows a depolarizing shift in the reversal potential of $Hcn1^{M294L}$ neurons (n = 14) compared to wild-type (n = 12), $^*P < 0.0001$. (**C**) *I–V* relationship for I_h from $Hcn1^{M294L}$ neurons (n = 5 wild-type, 5 $Hcn1^{M294L}$) shows minimal rectification. (**D**) The activation time constant (tau) of I_h in $Hcn1^{M294L}$ neurons is substantially faster and shows substantially weaker voltage dependence compared to wild-type (n = 5 wild-type, 5 $Hcn1^{M294L}$).

lacked voltage dependence (Fig. 5D). These findings recapitulated observations in oocytes (Fig. 4D and E). In summary, the disease variant caused a non-selective cation 'leak' HCN1 channel at more depolarized potentials.

Layer V pyramidal neurons from $Hcn1^{M294L}$ mice are hyperexcitable

HCN1 protein localization to the apical dendrites of layer V neurons appeared normal in the $Hcn1^{M294L}$ mouse (Fig. 6A).[26,27] Neurons from $Hcn1^{M294L}$ mice had reduced I_h-mediated sag (Fig. 6B and C), consistent with the reduced voltage sensitivity of the mutated channel (Figs 4 and 5). The RMP of neurons from $Hcn1^{M294L}$ mice was significantly more depolarized than that of neurons from wild-type mice (Fig. 6D and E). The depolarized RMP was also observed for $Hcn1^{M294L}$ neurons in the presence of NMDA, AMPA and $GABA_A$ receptor blockers (Fig. 6F) ruling out an influence of synaptic transmission on this phenomenon. ZD 7288 significantly hyperpolarized the RMP of both $Hcn1^{M294L}$ and wild-type neurons (Fig. 6G). This provided further evidence that I_h is active at the depolarized RMP seen in $Hcn1^{M294L}$ neurons, and that a proportion of the depolarized RMP of these cells can be attributed to aberrant current flow through the mutated HCN1 channel.

Next, we looked at the effect of the observed depolarized RMP on AP output. When measured from rest, neurons from $Hcn1^{M294L}$ mice had a significant left-shift in rheobase (Fig. 6H–J). There were no differences in the area under the *i–o* curve, suggesting no change in gain (Fig. 6K).

Effect of the Hcn1 M294L variant on input resistance of layer V pyramidal neurons

Given the importance of HCN1-mediated I_h in setting Rm in layer V pyramidal neurons,[28] we explored the impact of the Hcn1 M294L variant on this parameter. Interestingly, there was no significant difference in Rm between wild-type and $Hcn1^{M294L}$ layer V neurons at their respective RMP (Fig. 7A). To investigate this further, we used voltage clamp to measure Rm at a given holding potential. Rm measured at –70 mV was not significantly different between wild-type and $Hcn1^{M294L}$ layer V neurons (Fig. 7B). In contrast, Rm measured at –50 mV was significantly lower for $Hcn1^{M294L}$ layer V neurons (Fig. 7C) with the difference normalized by ZD 7288 (Fig. 7D). These findings are consistent with the notion that at more depolarized membrane potentials, Hcn1 channels are closed in wild-type, but remain open in $Hcn1^{M294L}$ neurons and thus contribute to lowering input resistance.

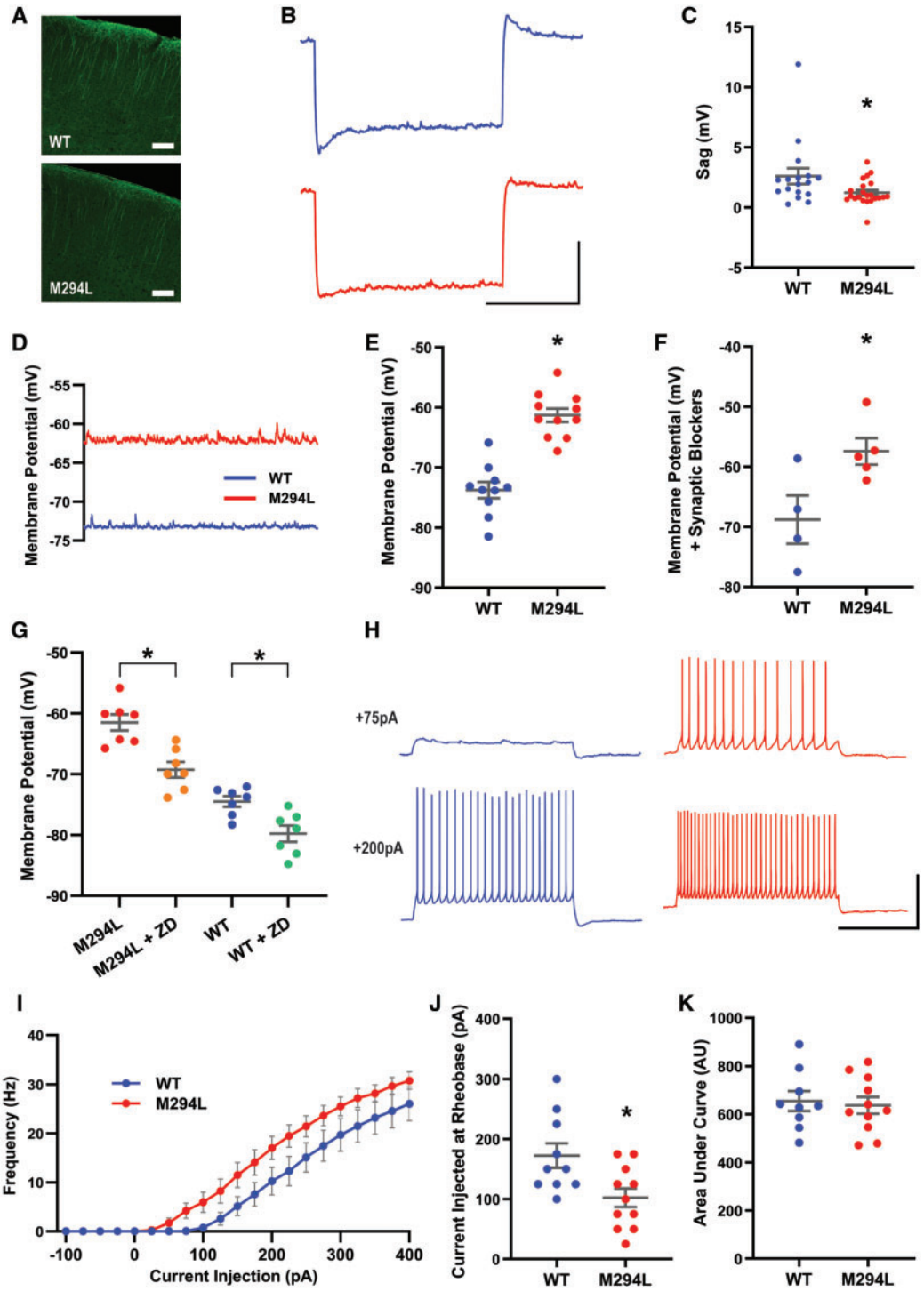

Figure 6 Layer V pyramidal neurons from Hcn1^{M294L} mice were hyperexcitable. (**A**) HCN1 protein staining of cortex from a wild-type mouse (*top*) and an Hcn1^{M294L} mouse (*bottom*), showing the expected predominant localization to the apical dendrites in both genotypes (scale bar = 100 μm). (**B**) Average of sag traces obtained from cells from wild-type mice (*top*, blue, n = 17) and cells from Hcn1^{M294L} mice (*bottom*, red, n = 22) (scale bar = 1 s, 5 mV). Layer V slice electrophysiology experiments were conducted on tissue from n = 7 wild-type and 8 Hcn1^{M294L} mice. (**C**) Sag is significantly reduced in layer V neurons from Hcn1^{M294L} mice (n = 17 wild-type, 22 Hcn1^{M294L}), *P = 0.03. (**D**) Example current clamp gap-free recordings from a layer V neuron from an Hcn1^{M294L} mouse (red) and from a wild-type mouse (blue) in the absence of any holding current. (**E**) Layer V neurons from Hcn1^{M294L} mice displayed a significantly depolarized resting membrane potential compared to layer V neurons from wild-type mice (n = 10 wild-type, 11 Hcn1^{M294L}), *$P < 0.0001$. (**F**) In the presence of the synaptic blocking drugs AP5, NBQX and picrotoxin, layer V neurons from Hcn1^{M294L} mice remained more depolarized than neurons from wild-type mice (n = 4 wild-type, 5 Hcn1^{M294L}), *P = 0.03. (**G**) The HCN channel blocking drug ZD 7288 caused a significant hyperpolarization of the RMP in both Hcn1^{M294L} neurons (n = 7, *P = 0.0008) and wild-type neurons (n = 7, *P = 0.0005). (**H**) Representative AP firing patterns in response to 2 s injections of +75 pA (*top*) and +200 pA (*bottom*) current in layer V neurons from wild-type (*left*, blue) and Hcn1^{M294L} (*right*, red) mice (scale bar = 1 s, 50 mV). (**I**) Summary of i–o data showed a left-shift in the input-output relationship in Hcn1^{M294L} layer V neurons compared to wild-type neurons (n = 10 wild-type, 11 Hcn1^{M294L}). (**J**) Rheobase was left-shifted in layer V neurons from Hcn1^{M294L} mice (n = 10 wild-type, 11 Hcn1^{M294L}), *P = 0.01. (**K**) There was no significant difference in gain, as measured by area under the curve in the 15 sweeps starting from the sweep immediately prior to rheobase, between layer V neurons from wild-type and Hcn1^{M294L} mice (n = 9 wild-type, 11 Hcn1^{M294L}), P = 0.7.

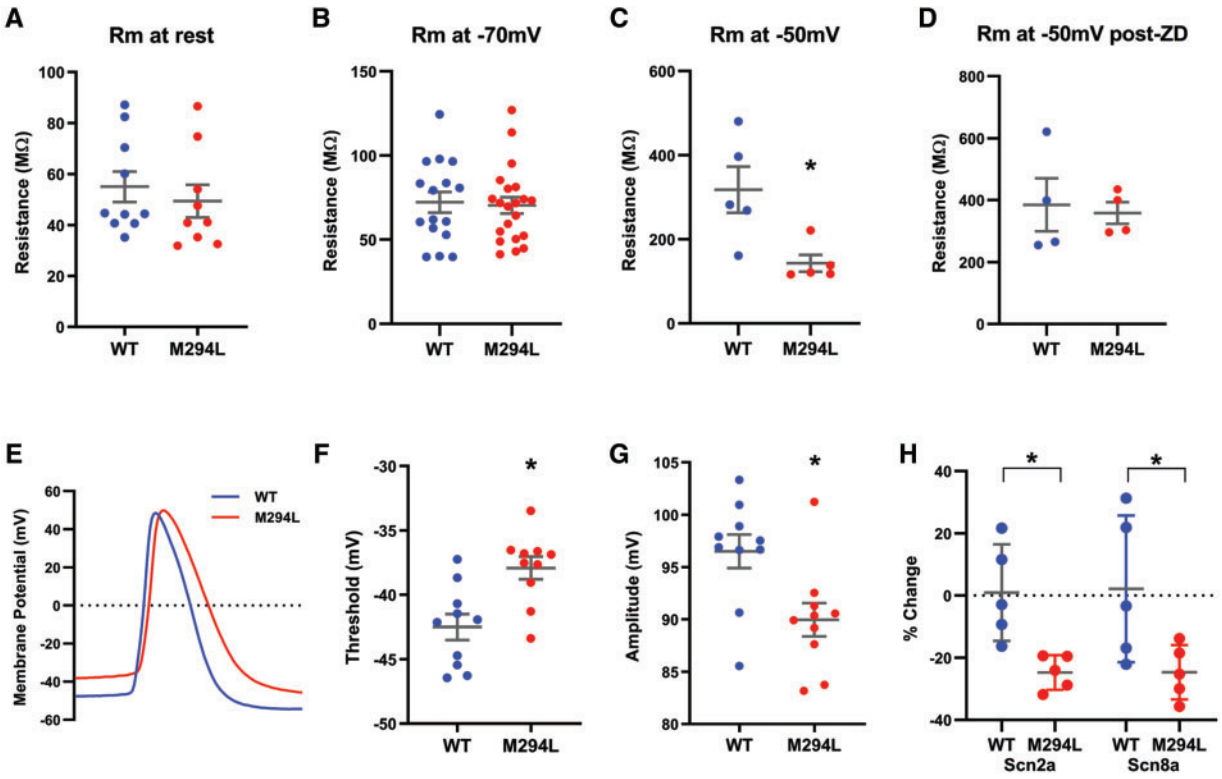

Figure 7 Input resistance and AP properties of layer V pyramidal neurons from Hcn1^{M294L} mice. (**A**) There was no significant difference in input resistance between wild-type (WT) and Hcn1^{M294L} neurons when measured from rest (n = 10 wild-type, 9 Hcn1^{M294L}), P = 0.5. (**B**) There was no significant difference in input resistance between wild-type and Hcn1^{M294L} neurons at a holding potential of –70 mV (n = 16 wild-type, 21 Hcn1^{M294L}), P = 0.8. (**C**) Hcn1^{M294L} neurons had a significantly lower input resistance than wild-type neurons at a holding potential of –50 mV (n = 5 wild-type, 5 Hcn1^{M294L}), *P = 0.02. (**D**) After the application of ZD 7288, there was no significant difference in input resistance between WT and Hcn1^{M294L} neurons at a holding potential of –50 mV (n = 4 wild-type, 4 Hcn1^{M294L}), P = 0.8. (**E**) Representative raw traces of the first AP fired at rheobase in a layer V neuron from a wild-type mouse (blue) and from an Hcn1^{M294L} mouse (red). (**F**) Layer V neurons from Hcn1^{M294L} mice had a significantly depolarized threshold for AP firing (n = 10 wild-type, 10 Hcn1^{M294L}), *P = 0.003. (**G**) Layer V neurons from Hcn1^{M294L} mice had a significantly reduced AP amplitude (n = 10 wild-type, 10 Hcn1^{M294L}), *P = 0.01. (**H**) Expression of *Scn2a* mRNA in cortical tissue was significantly reduced in Hcn1^{M294L} mice (n = 5 wild-type, 5 Hcn1^{M294L}), *P = 0.008. Expression of *Scn8a* mRNA in cortical tissue was significantly reduced in Hcn1^{M294L} mice (n = 5 wild-type, 5 Hcn1^{M294L}), *P = 0.04.

Hcn1^{M294L} neurons displayed no significant difference in sPSC amplitude or inter-event interval

We measured sPSCs from wild-type and Hcn1^{M294L} layer V neurons as a marker of local neuronal network excitability. No significant differences in sPSC amplitude were observed [25th percentile difference: –10.8, 95% confidence interval (CI) = –59.9 to 38.3, P = 0.7; median difference: –1.6, 95% CI = –6.2 to 3.0, P = 0.5; 75th percentile difference: –0.6, 95% CI = –2.4 to 1.2, P = 0.5], while inter-event intervals in sPSCs from Hcn1^{M294L} neurons were numerically shorter (hazard ratio = 0.7, 95% CI = 0.5 to 1.1, P = 0.2) with the difference not reaching statistical significance (Supplementary Fig. 1). These data suggest that there are no overt changes in synaptic transmission in Hcn1^{M294L} neurons.

Layer V pyramidal neurons from Hcn1^{M294L} mice show adaptation in action potential properties

APs from Hcn1^{M294L} layer V neurons measured from rest showed altered morphology, including depolarized threshold and reduced amplitude compared to wild-type (Fig. 7E–G and Supplementary Fig. 2). We also measured the firing properties of neurons 'clamped' at –70 mV. Rheobase for Hcn1^{M294L} neurons was no longer significantly different from wild-type (Supplementary Fig. 3A and B), consistent with the idea that the hyperexcitability of the Hcn1^{M294L} cells results from their depolarized RMP. Morphological changes in APs from Hcn1^{M294L} layer V neurons measured at –70 mV were similar to those changes recorded from rest, with APs being smaller and slower than those from wild-type neurons (Supplementary Fig. 3C–G). These data suggest that the observed differences in AP morphology and output result from an intrinsic change in the properties of voltage-activated sodium channels, rather than altered availability of these channels due to the depolarized RMP of Hcn1^{M294L} neurons.

To probe this, we conducted quantitative PCR on cortical tissue from wild-type and Hcn1^{M294L} mice to study mRNA levels of the voltage-gated sodium channels $Na_v1.2$ and $Na_v1.6$, which are critical for AP generation at the axon initial segment in layer V pyramidal neurons.[29] mRNA expression levels of both *Scn2a* and *Scn8a* were significantly reduced in Hcn1^{M294L} mice (Fig. 7H). This suggests that reduced expression of $Na_v1.2$ and $Na_v1.6$ channels may underlie the altered AP threshold and reduced AP amplitude seen in Hcn1^{M294L} neurons. Quantitative PCR on cortical tissue revealed no suggestions of transcriptional regulation of HCN channels in Hcn1^{M294L} mice, with *Hcn1* and *Hcn2* mRNA levels similar to wild-type (Supplementary Fig. 4). This argues against a major role of altered HCN channel transcription on our observations.

CA1 neurons from Hcn1^{M294L} mice are hyperexcitable

Similar to observations in layer V neurons, I_h-mediated sag was reduced in hippocampal CA1 neurons from Hcn1^{M294L} mice (Fig. 8A

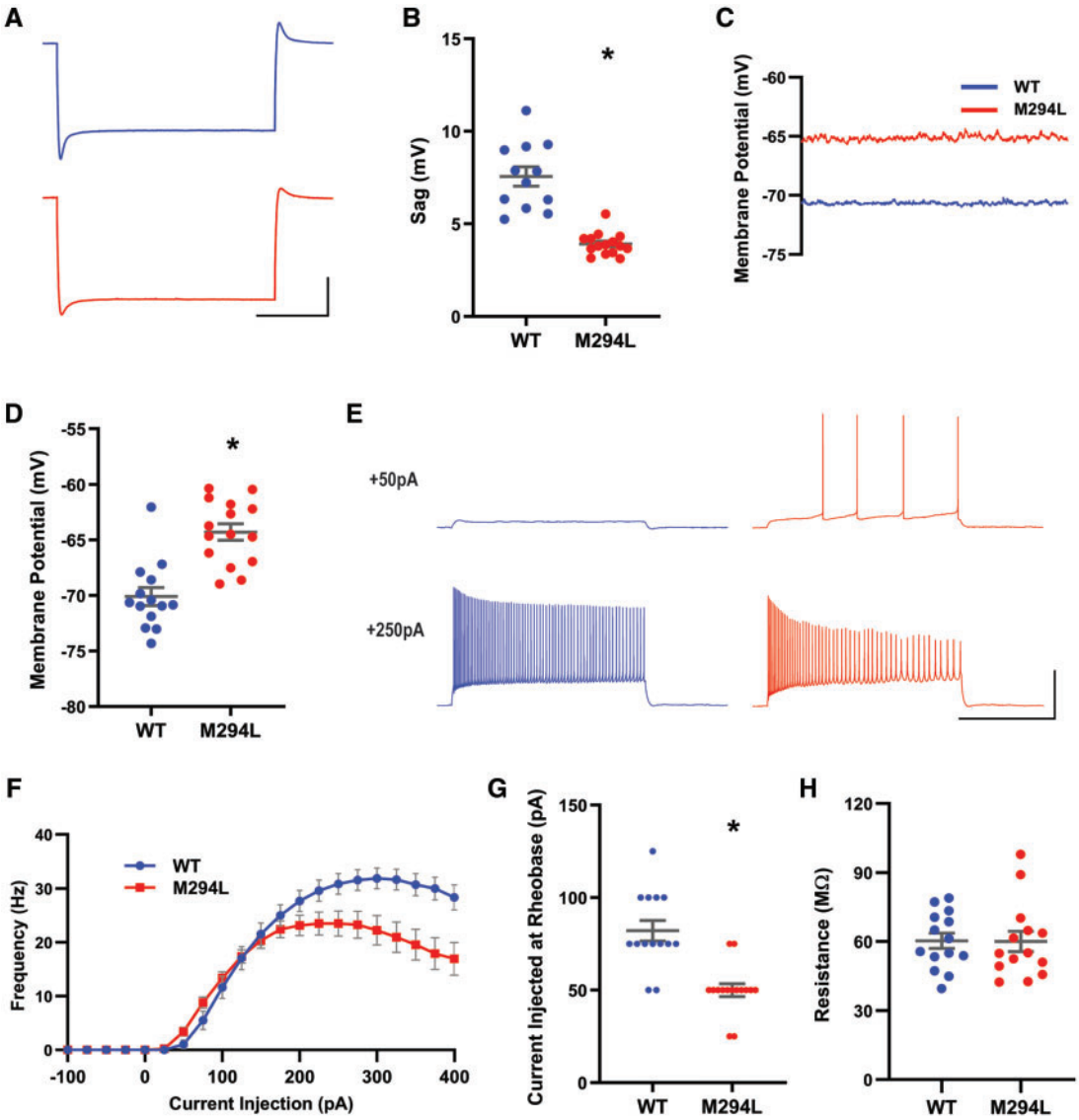

Figure 8 CA1 neurons from Hcn1^{M294L} mice were hyperexcitable. (**A**) Average of sag traces obtained from cells from wild-type (WT) mice (*top*, blue, *n* = 12) and cells from Hcn1^{M294L} mice (*bottom*, red, *n* = 15) (scale bar = 1 s, 10 mV). Slice electrophysiology experiments were conducted on tissue from *n* = 2 wild-type and 2 Hcn1^{M294L} mice. (B) Sag is significantly reduced in CA1 neurons from Hcn1^{M294L} mice (*n* = 12 wild-type, 15 Hcn1^{M294L}), *$P < 0.0001$. (**C**) Example current clamp gap-free recordings from a CA1 neuron from an Hcn1^{M294L} mouse (red) and from a wild-type mouse (blue) in the absence of any holding current. (**D**) CA1 neurons from Hcn1^{M294L} mice displayed a significantly depolarized resting membrane potential compared to CA1 neurons from wild-type mice (*n* = 14 wild-type, 15 Hcn1^{M294L}), *$P < 0.0001$. (**E**) Representative AP firing patterns in response to 2 s injections of +50 pA (*top*) and +250 pA (*bottom*) current in CA1 neurons from wild-type (*left*, blue) and Hcn1^{M294L} (*right*, red) mice (scale bar = 1 s, 50 mV). (**F**) Summary of i–o data showed a left-shift in rheobase and an earlier firing collapse in Hcn1^{M294L} CA1 neurons compared to wild-type neurons (*n* = 14 wild-type, 15 Hcn1^{M294L}). (**G**) Rheobase was left-shifted in CA1 neurons from Hcn1^{M294L} mice (*n* = 14 wild-type, 15 Hcn1^{M294L}), *$P < 0.0001$. (**H**) There was no significant difference in input resistance between wild-type and Hcn1^{M294L} CA1 neurons when measured from rest (*n* = 14 wild-type, 14 Hcn1^{M294L}), $P = 0.6$.

and B), and the RMP of these neurons was significantly depolarized compared to wild-type (Fig. 8C and D). When measured from rest, a significant left-shift in rheobase was observed in CA1 neurons from Hcn1^{M294L} mice, although some collapse in AP firing was observed at higher depolarizing current injections (Fig. 8E–G). APs from Hcn1^{M294L} CA1 neurons also showed a trend towards similar morphological features as those from layer V neurons (Supplementary Fig. 5). In line with findings in layer V neurons, there was no significant difference in Rm between wild-type and Hcn1^{M294L} CA1 neurons when measured at rest in current clamp (Fig. 8H).

In summary, our data support a model of hyperexcitability whereby the aberrant HCN1 cation 'leak' channel causes a depolarized RMP in both layer V and CA1 pyramidal neurons, consequently contributing to a left-shift in rheobase.

Discussion

In this study we have investigated the mechanisms underlying *HCN1* DEE. We characterized the Hcn1^{M294L} mouse model and demonstrated that it recapitulated the major phenotypic aspects of human *HCN1* DEE associated with the M305L variant. These included spontaneous seizures, susceptibility to heat-induced seizures, lower body weight, epileptiform ECoG activity which improved with sodium valproate and worsened with lamotrigine, and a learning deficit. Functional analysis revealed that the

pathogenic variant disrupts the voltage dependence of the HCN1 channel, rendering the channel constitutively open and resulting in aberrant cation 'leak' with consequent depolarization of pyramidal neurons.

Our functional analysis of the HCN1 M305L channel qualitatively recapitulated data obtained from expression in HEK293 cells,[5] including an almost instantaneous change in macroscopic current in response to voltage steps, absence of tail currents, and a significant reduction in inward rectification. The unchanged permeation of Na^+ and K^+ through variant and wild-type channels suggests that pore function is unaffected. I_h in layer V neurons from Hcn1^{M294L} mice had rapid activation kinetics and minimal inward rectification, essentially recapitulating the biophysical parameters observed in oocytes. These results are consistent with a mechanism whereby the M305L variant uncouples the channel's voltage sensor from the pore opening, resulting in a cation 'leak' channel that lacks the characteristic activation kinetics of wild-type HCN1. Functional analysis of other *HCN1* DEE variants, including G391S, I397L, and heteromeric expression of G391D, also predicted that more HCN1-mediated current would occur at depolarized potentials, albeit to a variable extent.[5] This suggests that there may be similar pathogenic mechanisms underlying a proportion of *HCN1* DEEs and positions the Hcn1^{M294L} mouse as a representative preclinical model of HCN1 disease more generally.

As a consequence of the cation 'leak', neurons from Hcn1^{M294L} mice were significantly more depolarized at rest than wild-type, by ~6 mV in CA1 neurons and a remarkable ~12 mV in layer V neurons. The broad-spectrum HCN channel blocker, ZD 7288, significantly hyperpolarized layer V Hcn1^{M294L} neurons from rest. This strongly suggests that aberrant I_h was contributing to the depolarized RMP. However, ZD 7288 was not able to fully normalize RMP back to wild-type levels. While we believe that cation 'leak' through the aberrantly functioning HCN1 channel is the primary driver of depolarization, it remains possible that dysregulation or adaptation of other ion channels could also contribute.

We saw a significant left-shift in rheobase due to the depolarized RMP in both layer V and CA1 pyramidal neurons, providing a consistent mechanistic explanation for neuronal hyperexcitability. Interestingly, the observed shift in rheobase of layer V neurons was relatively small given the magnitude of RMP depolarization. This could be explained, at least in part, by the compensatory depolarized shift in AP threshold. This shift in threshold was also seen when layer V neurons were 'clamped' at –70 mV, indicating that it is unlikely to result from a reduction in sodium channel availability due to depolarization-mediated inactivation. Our qPCR results revealed a reduction in the expression of *Scn2a* and *Scn8a* mRNA, and therefore presumably protein, in cortical tissue that could be part of this compensatory mechanism.

Evidently, Hcn1^{M294L} neurons have adapted in a way that allows them to maintain their ability to fire APs at a relatively normal rate, despite their significantly depolarized RMP. In particular, the *i-o* gain for layer V Hcn1^{M294L} neurons is surprisingly similar to wild-type. This has been achieved, at least in part, through the aforementioned adaptive changes in AP threshold. Another noteworthy finding is the lack of significant difference in input resistance between wild-type and Hcn1^{M294L} cells at rest, and the fact that we observed no change in the amplitude of sPSCs in Hcn1^{M294L} cells. We propose that this finding can at least partially be explained by Hcn1 channels remaining open and passing current at rest in both wild-type and Hcn1^{M294L} cells. Other contributing factors, such as altered morphology of mutant neurons[30] or changes in background K^+ conductances may also be present. Adaptations such as these, which prevent substantial changes in gain and input resistance at rest in Hcn1^{M294L} cells, are likely critical to why Hcn1^{M294L} mice can survive and function.

Despite these adaptations, Hcn1^{M294L} mice display clear deficits including a reduced ability to encode and recall longer-term spatial reference memories. The underlying basis of this is unclear. However, HCN1 channels are highly expressed in the dendrites of pyramidal cells[26,27] where they are known to play integral roles in synaptic summation.[27,31–33] The observed learning deficit may reflect a reduction in the ability of Hcn1^{M294L} neurons to appropriately integrate incoming information at the dendrites, although this would require additional experimentation to explore.

We observed only rare spontaneous tonic-clonic seizures in Hcn1^{M294L} mice. However, there were striking morphological changes in the brains of adult mice consistent with temporal lobe epilepsy.[23,24] Additionally, ECoG spiking occurred in all Hcn1^{M294L} mice recorded, providing clear evidence of an epileptic brain. The reduction in ECoG spikes following administration of sodium valproate was consistent with the clinical efficacy of this drug in a patient with *HCN1* DEE due to the M305L variant. Equally, increased spiking and the triggering of seizures by lamotrigine recapitulated clinical observations, providing face validity for the mouse model. Potential explanations for this observation include lamotrigine further enhancing the already aberrant I_h,[32] or blocking voltage-gated sodium channels in inhibitory neurons causing a disinhibitory effect similar to that seen in *SCN1A* epilepsies.[3,34]

The mechanistic basis underlying *HCN1* DEE revealed in this study gives insight into therapeutic approaches that may be effective for this disease. For example, blocking the aberrant HCN1 channel or normalizing RMP may help to restore normal functionality. The Hcn1^{M294L} mouse provides an excellent model in which to screen potential treatments, including small molecules and gene therapies, which could offer these effects. However, neurons of these individuals have evidently adapted to their depolarized condition. This highlights the likely importance of early intervention to minimize the occurrence of adaptive changes during development, and also suggests that therapies may need to be introduced slowly to allow the brain to readjust.

In summary, we have demonstrated a gain of aberrant function mechanism in the HCN1 channel which underlies neuronal hyperexcitability in *HCN1* DEE due to the M305L pathogenic variant. The Hcn1^{M294L} mouse recapitulated many of the major aspects of human *HCN1* DEE and showed clear face validity with respect to drug responses, making it a strong preclinical model for disease caused by gain of aberrant function variants.

Acknowledgements

We thank the patient and her family for participating in our research. We would like to acknowledge Marie Phillips for providing the mutagenized oocyte construct and for reading and providing feedback on the manuscript. We are grateful to Anastasia Barnett for excellent technical assistance. The Hcn1^{M294L} mouse line was produced by the Monash University node of the Australian Phenomics Network (APN). The APN is supported by the Australian Government through the National Collaborative Research Infrastructure Strategy (NCRIS) Program.

Funding

This work was supported by National Health and Medical Research Council (NHMRC) Program Grant (10915693) to S.F.B., I.E.S., S.P. and C.A.R., and from the National Institutes of Health (NIH) grants NINDS R01-NS106983 and NINDS R01-NS109366 to B.S. L.E.B. acknowledges the support of an Australian Government Research Training Program Scholarship. The Florey Institute of Neuroscience and Mental Health is supported by Victorian State Government infrastructure funds.

Competing interests

I.E.S. may accrue future revenue on pending patent WO2009/086591: Diagnostic And Therapeutic Methods For EFMR (Epilepsy And Mental Retardation Limited To Females); has a patent for SCN1A testing held by Bionomics Inc and licensed to various diagnostic companies (WO/2006/133508); she has a patent for a molecular diagnostic/therapeutic target for benign familial infantile epilepsy (BFIE) [PRRT2] WO/2013/059884 with royalties paid. She has served on scientific advisory boards for UCB, Eisai, GlaxoSmithKline, BioMarin, Nutricia, Rogcon and Xenon Pharmaceuticals; has received speaker honoraria from GlaxoSmithKline, UCB, BioMarin, Biocodex and Eisai; has received funding for travel from UCB, Biocodex, GlaxoSmithKline, Biomarin and Eisai; has served as an investigator for Zogenix, Zynerba, Ultragenyx, GW Pharma, UCB, Eisai, Anavex Life Sciences and Marinus; and has consulted for Zynerba Pharmaceuticals, Atheneum Partners, Ovid Therapeutics and UCB. The remaining authors report no competing interests.

Supplementary material

Supplementary material is available at *Brain* online.

References

1. Fisher RS, Acevedo C, Arzimanoglou A, et al. ILAE official report: A practical clinical definition of epilepsy. *Epilepsia*. 2014;55(4):475–482.
2. Thomas RH, Berkovic SF. The hidden genetics of epilepsy - A clinically important new paradigm. *Nat Rev Neurol*. 2014;10(5):283–292.
3. Oyrer J, Maljevic S, Scheffer IE, Berkovic SF, Petrou S, Reid CA. Ion channels in genetic epilepsy: From genes and mechanisms to disease-targeted therapies. *Pharmacol Rev*. 2018;70(1):142–173.
4. Bonzanni M, DiFrancesco JC, Milanesi R, et al. A novel de novo HCN1 loss-of-function mutation in genetic generalized epilepsy causing increased neuronal excitability. *Neurobiol Dis*. 2018;118:55–63.
5. Marini C, Porro A, Rastetter A, et al. HCN1 mutation spectrum: from neonatal epileptic encephalopathy to benign generalized epilepsy and beyond. *Brain*. 2018;141(11):3160–3178.
6. Nava C, Dalle C, Rastetter A, et al. De novo mutations in HCN1 cause early infantile epileptic encephalopathy. *Nat Genet*. 2014;46(6):640–645.
7. Dibbens LM, Reid CA, Hodgson B, et al. Augmented currents of an HCN2 variant in patients with febrile seizure syndromes. *Ann Neurol*. 2010;67(4):542–546.
8. Becker F, Reid CA, Hallmann K, et al. Functional variants in HCN4 and CACNA1H may contribute to genetic generalized epilepsy. *Epilepsia Open*. 2017;2(3):334–342.
9. Campostrini G, DiFrancesco JC, Castellotti B, et al. A loss-of-function HCN4 mutation associated with familial benign myoclonic epilepsy in infancy causes increased neuronal excitability. *Front Mol Neurosci*. 2018;11:269.
10. Li M, Maljevic S, Phillips AM, et al. Gain-of-function HCN2 variants in genetic epilepsy. *Hum Mutat*. 2018;39(2):202–209.
11. Biel M, Wahl-Schott C, Michalakis S, Zong X. Hyperpolarization-activated cation channels: from genes to function. *Physiol Rev*. 2009;89(3):847–885.
12. Parrini E, Marini C, Mei D, et al. Diagnostic targeted resequencing in 349 patients with drug-resistant pediatric epilepsies identifies causative mutations in 30 different genes. *Hum Mutat*. 2017;38(2):216–225.
13. Scheffer IE, Berkovic S, Capovilla G, et al. ILAE classification of the epilepsies: Position paper of the ILAE Commission for Classification and Terminology. *Epilepsia*. 2017;58(4):512–521.
14. Zhang YH, Burgess R, Malone JP, et al. Genetic epilepsy with febrile seizures plus: Refining the spectrum. *Neurology*. 2017;89(12):1210–1219.
15. Reid CA, Phillips AM, Petrou S. HCN channelopathies: pathophysiology in genetic epilepsy and therapeutic implications. *Br J Pharmacol*. 2012;165(1):49–56.
16. Santoro B, Baram TZ. The multiple personalities of h-channels. *Trends Neurosci*. 2003;26(10):550–554.
17. Reid CA, Kim T, Phillips AM, et al. Multiple molecular mechanisms for a single GABAA mutation in epilepsy. *Neurology*. 2013;80(11):1003–1008.
18. Clements JD, Bekkers JM. Detection of spontaneous synaptic events with an optimally scaled template. *Biophys J*. 1997;73(1):220–229.
19. Butler LS, Silva AJ, Abeliovich A, Watanabe Y, Tonegawa S, McNamara JO. Limbic epilepsy in transgenic mice carrying a Ca2 + /calmodulin-dependent kinase II α-subunit mutation. *Proc Natl Acad Sci U S A*. 1995;92(15):6852–6855.
20. Racine RJ. Modification of seizure activity by electrical stimulation. II. Motor seizure. *Electroencephalogr Clin Neurophysiol*. 1972;32(3):281–294.
21. Stringer JL. Repeated seizures increase GFAP and vimentin in the hippocampus. *Brain Res*. 1996;717(1-2):147–153.
22. Marksteiner J, Ortler M, Bellmann R, Sperk G. Neuropeptide Y biosynthesis is markedly induced in mossy fibers during temporal lobe epilepsy of the rat. *Neurosci Lett*. 1990;112(2-3):143–148.
23. Houser CR. Granule cell dispersion in the dentate gyrus of humans with temporal lobe epilepsy. *Brain Res*. 1990;535(2):195–204.
24. Magagna-Poveda A, Moretto JN, Scharfman HE. Increased gyrification and aberrant adult neurogenesis of the dentate gyrus in adult rats. *Brain Struct Funct*. 2017;222(9):4219–4237.
25. Sharma S, Rakoczy S, Brown-Borg H. Assessment of spatial memory in mice. *Life Sci*. 2010;87(17-18):521–536.
26. Santoro B, Grant SGN, Bartsch D, Kandel ER. Interactive cloning with the SH3 domain of N-src identifies a new brain specific ion channel protein, with homology to Eag and cyclic nucleotide-gated channels. *Proc Natl Acad Sci U S A*. 1997;94(26):14815–14820.
27. Williams SR, Stuart GJ. Site independence of EPSP time course is mediated by dendritic Ih in neocortical pyramidal neurons. *J Neurophysiol*. 2000;83(5):3177–3182.
28. Thuault SJ, Malleret G, Constantinople CM, et al. Prefrontal cortex HCN1 channels enable intrinsic persistent neural firing and executive memory function. *J Neurosci*. 2013;33(34):13583–13599.
29. Hu W, Tian C, Li T, Yang M, Hou H, Shu Y. Distinct contributions of Na(v)1.6 and Na(v)1.2 in action potential initiation and backpropagation. *Nat Neurosci*. 2009;12(8):996–1002.
30. Reid CA, Leaw B, Richards KL, et al. Reduced dendritic arborization and hyperexcitability of pyramidal neurons in a Scn1b-based model of Dravet syndrome. *Brain*. 2014;137(Pt 6):1701–1715.
31. Magee JC. Dendritic lh normalizes temporal summation in hippocampal CA1 neurons. *Nat Neurosci*. 1999;2(6):508–514.
32. Poolos NP, Migliore M, Johnston D. Pharmacological upregulation of h-channels reduces the excitability of pyramidal neuron dendrites. *Nat Neurosci*. 2002;5(8):767–774.
33. Tsay D, Dudman JT, Siegelbaum SA. HCN1 channels constrain synaptically evoked Ca2 + spikes in distal dendrites of CA1 pyramidal neurons. *Neuron*. 2007;56(6):1076–1089.
34. Yu FH, Mantegazza M, Westenbroek RE, et al. Reduced sodium current in GABAergic interneurons in a mouse model of severe myoclonic epilepsy in infancy. *Nat Neurosci*. 2006;9(9):1142–1149.
35. Lee CH, MacKinnon R. Structures of the human HCN1 hyperpolarization-activated channel. *Cell*. 2017;168(1-2):111–120.e11.